SCIENCE CHINA
Information Sciences

• RESEARCH PAPER •

June 2015, Vol. 58 062402:1–062402:7
doi: 10.1007/s11432-015-5283-0

Doping profile modification approach of the optimization of HfO_x based resistive switching device by inserting AlO_x layer

HOU Yi, CHEN Bing, CHEN Zhe, ZHANG FeiFei, LIU LiFeng*,
KANG JinFeng & CHENG YuHua

Institute of Microelectronics, Peking University, Beijing 100871*, China*

Received May 4, 2014; accepted October 10, 2014 ; published online April 17, 2015

Abstract HfO_x based resistive switching devices with thin AlO_x layer inserted between HfO_x and TiN top electrode (TE) and Pt bottom electrode (BE) were fabricated respectively. Both devices show robust bipolar resistive switching phenomenon. Experimental result reveals that $TiN/AlO_x/HfO_x/Pt$ device with appropriately thick HfO_x film shows significant enhancement in performance as compared with other samples, having lower voltage and excellent uniformity. The role of inserted AlO_x layer and thickness of HfO_x film on resistive switching properties are discussed and clarified through comparative experiments, which is considered to be a doping effect. The experimental result is consistent with the model where resistive switching happens near TiN top electrode (TE) due to partial rupture and reconstruction of conducting filaments (CFs) assisted by the doping. The different doping profiles near top electrode of the samples were confirmed by XPS depth analysis. This work provides detailed information about the optimization of HfO_x based resistive switching device by a doping profile modification approach.

Keywords RRAM, uniformity, switching voltage, HfO_x, AlO_x, doping

Citation Hou Y, Chen B, Chen Z, et al. Doping profile modification approach of the optimization of HfO_x based resistive switching device by inserting AlO_x layer. Sci China Inf Sci, 2015, 58: 062402(7), doi: 10.1007/s11432-015-5283-0

1 Introduction

Resistance random access memory (RRAM) has drawn research community's attention as a candidate for future non-volatile memory in recent years [1–4]. Major advantages of RRAM include high switching speed [5], low power operation [6], and potential in further scaling [7], etc. Despite the flexibility in material option [8–11], binary metal oxides, e.g., HfO_x, has been extensively studied in past years [7]. HfO_x based materials have been employed as gate dielectric in CMOS transistor fabrication, and TiN used as barrier layer against Cu diffusion in CMOS technology, which enabled $TiN/HfO_x/Pt$ structure to be CMOS compatible and one of the most mature resistive switching device so far. However, according to the filamentary nature of resistive switching phenomenon [12,13], random filament formation and rupture cause switching parameter dispersion such as resistance and operating voltage. Such parameter deviation

* Corresponding author (email: lfliu@pku.edu.cn)

is detrimental for the simplification of RRAM circuit design and reliability issue, and therefore should be carefully fabricated during RRAM designing. Doping has been proposed to be an effective approach to improve RRAM switching characteristics and various dopants have been employed such as Copper [14], Aluminium [15], Magnesium [16] and Nitrogen [17], etc. Our previous work [15] effectively lowered the device variation by embedding Al layers between electrodes and HfO_x before annealing during fabrication to form TiN/AlO_x/HfO_x/AlO_x/Pt structure. However, it provided insights only about introducing Al atoms in HfO_x resistive switching device resulting in improved uniformity and the detailed mechanism of the improvements induced by AlO_x inserting layer was not clarified. In this work, the resistive switching uniformity is further improved with a simpler bi-layer structure and the roles of Al doping profile between electrodes and HfO_x are further investigated and clarified through comparative experiments and electrical properties characterization.

2 Experiments

The RRAM devices with TiN/AlO_x/HfO_x/Pt and TiN/HfO_x/AlO_x/Pt (with different HfO_x film thickness)structure were fabricated to illustrate the roles of AlO_x insert layer and dependence on HfO_x film thickness (different doping profile). First, about 100 nm Pt with a 20 nm Ti adhesive layer was sputtered on SiO_2/Si substrates. Then, 3 nm Al/15 nm Hf was deposited in turn to form S1, 30 nm Hf/3 nm Al to form S2, 15 nm Hf/3 nm Al to form S3, respectively, and all of it was performed by Physical Vapor Deposition (PVD). Next, all samples were annealed at 600°C, in N_2 ambient for 10 min followed by O_2 ambient for 60 min. Finally, TiN top electrodes were sputtered and patterned. The fabricated samples participated in comparative experiments were schematically shown in Figure 1. Electrical characterizations were performed by Keithley 4200 analyzer with Pt bottom electrode grounded and voltages were applied on TiN top electrode.

3 Results and discussion

3.1 Forming process

The initial resistance states of the fresh samples are very high (GΩ), and an electroforming process is needed to activate the switching property. The forming process is interpreted to be equivalent to a soft dielectric breakdown [18]. We use current sweep mode in 4200 analyzer in this work, as shown in Figure 2. Significant reduction in forming current (I_{forming}) and maximum voltage during forming process(V_{forming}) are observed in S3 compared with S1 and S2. Meanwhile, S1 requires slightly lower I_{forming} and V_{forming} when comparing S1 with S2. We attributed S3's huge reduction in I_{forming} and V_{forming} to the doping profile induced by the AlO_x insert layer. First principle calculations have shown that Al atoms lower the formation energy (E_{V_o}) of oxygen vacancies (V_o) nearby [19]. Al atoms diffuse into HfO_x layer during PVD and post-deposition annealing process, and thus contribute to the formation of V_o based top-to-bottom percolation paths to complete dielectric soft breakdown. However, S1 and S2's doping profiles do not benefit much from the AlO_x insert layer during the forming process. As for S1, it should be noted that S1 and S3 are different in the deposition sequence of Al and Hf. S3 was fabricated by sputtering 15 nm Hf followed by 3 nm Al, the Al deposition process by PVD contributed to the injection and diffusion of Al atoms into Hf film similar to the mechanism of sputtering damage [20]. Meanwhile, S1 was fabricated by sputtering 3 nm Al at first, thus lost the chance of enhanced injection of Al atoms into Hf film during PVD, and therefore resulted in a lower Al doping level in HfO_x film after annealing process. Since it is the enhanced Al doping concentration that leads to the much lower I_{forming} and V_{forming} level, the different electrical characteristics of S1 and S3 can now be understood.

The forming voltage of S2 is larger than two times of S3's, shows the absence of AlO_x insert layer's advantageous doping effect in S2. It may be the influence of film thickness. There are two possible explanations. First, the Al atoms are limited in quantity due to the deposited Al film thickness, which leads to inadequate Al concentration in HfO_x film. Another explanation is the limited energy gain by Al

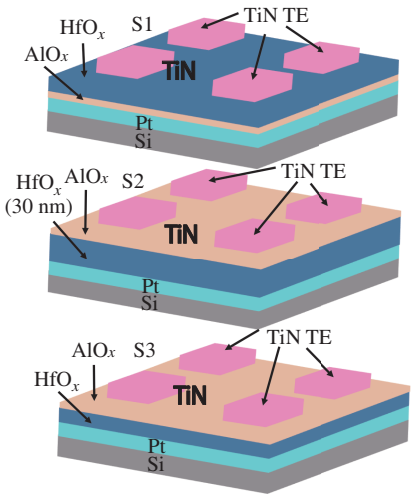

Figure 1 Schematic view of the fabricated resistive switching samples with AlO_x insert layer.

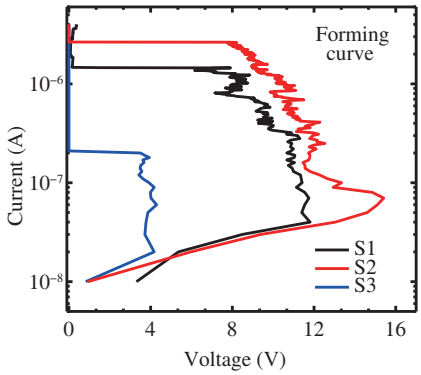

Figure 2 Initial forming process of the fabricated HfO_x based resistive switching devices.

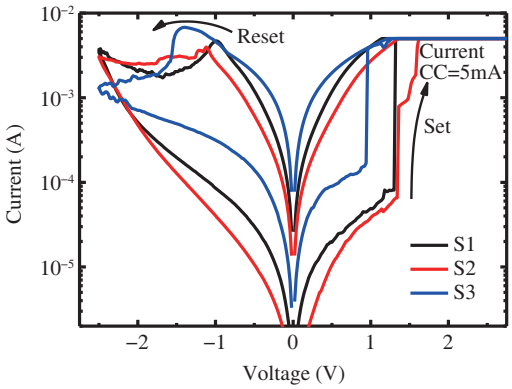

Figure 3 Initial forming process of the fabricated HfO_x based resistive switching devices.

atoms during PVD and annealing which results in limited depth of Al diffusion, in other words, the HfO_x film is too thick for Al atoms to diffuse from top to bottom. The V_o based percolation paths can hardly be built from top to bottom at a reduced E_{V_o} level induced by Al atoms. Both reasons may co-contribute to the high I_{forming} and V_{forming} in S2. Aforementioned analyses deduce that the differences between S1 S2 and S3 depend on Al doping profile and HfO_x layer thickness. Thicker HfO_x film and lower Al doping concentration require higher forming voltage and current to realize dielectric soft breakdown.

3.2 Resistive switching characteristics

Figure 3 shows the measured I-V curves of our samples after forming process using DC-sweep. A 5 mA compliance is introduced to avoid device hard breakdown during set process, while no current compliance is employed in the reset process. Typical bipolar resistive switching phenomenon is observed in all samples. The I-V of S1 and S2 are similar, but lower SET voltage (V_{SET}) is found in S3, indicating that different doping profile influences the switching characteristics of AlO_x/HfO_x bi-layer RRAM. In order to understand the current transport mechanisms in our comparative experiments, I-V curves of the samples in high resistance state (HRS) are exploited and fitted as shown in Figure 4. It can be noticed that the I-V curves of all three samples have two regions, the Ohmic like region ($I \propto V$) under low voltages and the Child's square-law region ($I \propto V^2$) under high voltages until an abrupt current jump to low resistance state (LRS), this is in good agreement with the prediction of trap controlled Space-Charge-Limited-Current (SCLC) current flow mechanism [21–23]. To verify the commercialization potential of

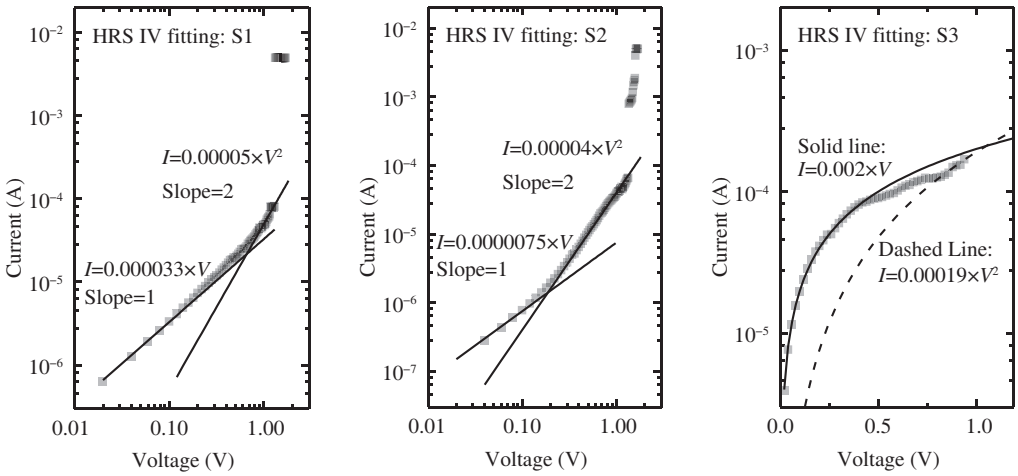

Figure 4 Fitted I-V curve in high resistance state of the samples, respectively.

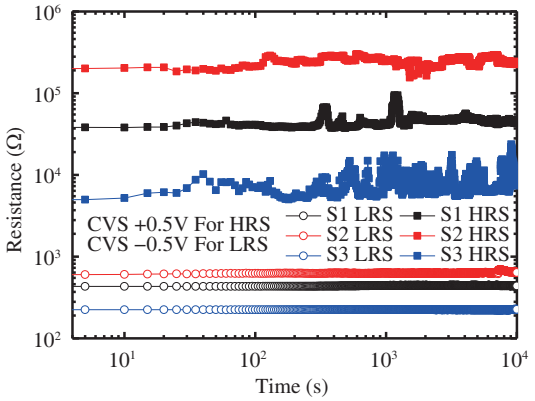

Figure 5 Retention properties of the samples, respectively.

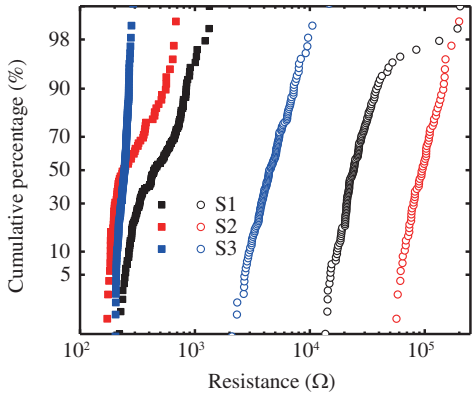

Figure 6 Measured resistance in high resistance state (HRS) and low resistance state (LRS) distribution within 128 cycles of the samples, respectively.

the samples in our experiment, data retention properties are characterized as shown in Figure 5. Both HRS and LRS of the samples remain stable after 10^4 s constant voltage stress. It is also worth mentioning that all the samples can switch in AC mode with 20 ns width voltage pulse, proving themselves to be promising in future memory application.

Uniformity parameters like resistance and operation voltage deviation are also studied in our comparative experiments. Figure 6 shows the distribution of resistance values in high resistance state (R_{HRS}) and low resistance state (R_{LRS}) measured by DC sweep mode for 128 continuous cycles. Figure 7 demonstrates the distribution of V_{SET} and V_{RESET} during the switching cycles. Suppressed resistance and operation voltage dispersion are observed in S3 unlike in S1 and S2.

Table 1 compares the key parameters of variations (standard deviation δ mean value μ) of R_{HRS}, R_{LRS}, V_{SET} and V_{RESET} in this work and literature [15]. It is deduced that the aforementioned difference in electric characteristics results from various Al doping profile induced by different fabrication process, especially the Al layer deposition moment. As depicted in Figure 8. S1 has its Al-rich region near Pt bottom electrode only, because Al was deposited first and S1 was deprived of injection or diffusion of Al in subsequent processes. However, S3, received adequate injection and diffusion during PVD and annealing process, and had its Al-rich region throughout the HfO_x resistive switching layer. S2 has its Al-rich region near TiN top electrode. As it is the oxygen vacancy that forms the conducting filaments during set process, the formation energy of oxygen vacancies (E_{V_o}) are significantly lowered in the vicinity of Al atoms, to facilitate formation of filaments.

Considering the reset process, it is well-known that TiN top electrode acts as good oxygen reservoir and

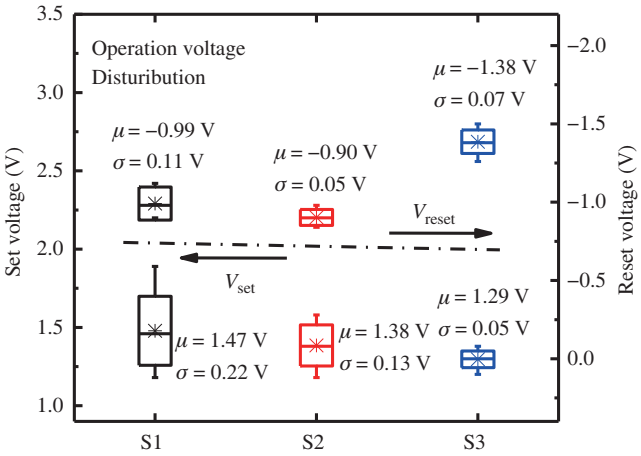

Figure 7 Statistical summary of resistive switching parameters during 128 continuous cycles in the samples.

Table 1 Comparison of uniformity parameters in this work with literature

Sample	Device structure	δ/μ R_{HRS} (%)	δ/μ R_{LRS} (%)	δ/μ V_{SET} (%)	δ/μ V_{RESET} (%)
S1	TiN/HfO_x/AlO_x/Pt	86.3	47.5	14.8	10.6
S2	TiN/AlO_x/HfO_x(30 nm)/Pt	29.7	46.2	9.4	5.6
S3	TiN/AlO_x/HfO_x/Pt	37.6	8.4	4.0	5.4
Yu et al. [15]	TiN/AlO_x/HfO_x/AlO_x/Pt	39.7	10.4	19.2	
Yu et al. [15]	TiN/HfO_x/Pt	70.7	76.2	29.4	

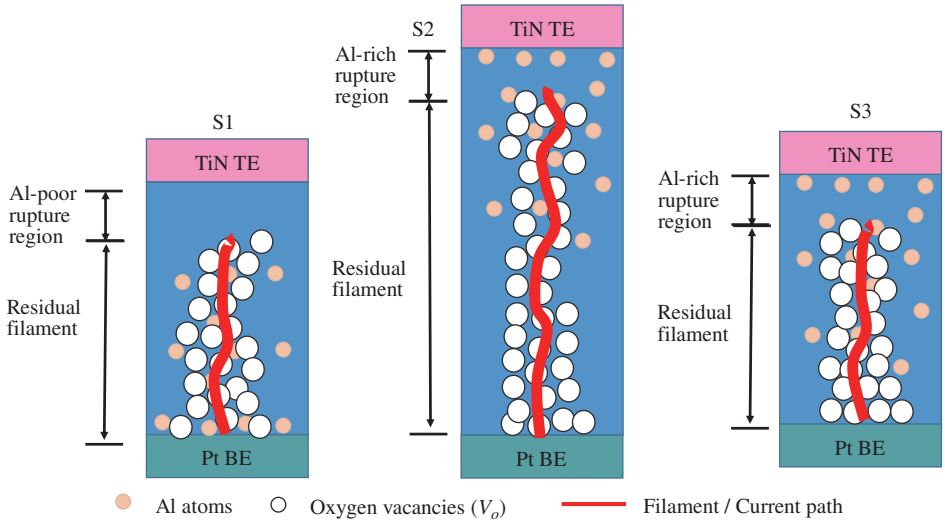

Figure 8 Schematic view of the proposed Al doping profile model. S1 had its Al-rich region near Pt bottom electrode (BE), S2 and S3 had their Al-rich regions near TiN top electrode (TE). The resistive switching phenomenon was due to the partial rupture and reconstruction of V_o based conducting filaments near TE. Al-rich rupture region guarantees an easier filament formation and ended up in uniform parameters.

can provide sufficient non-lattice oxygen ions to recover the oxygen vacancies to interrupt the filaments consisting of V_o [24]. As reset process is attributed to the exchange of oxygen ions between conducting filaments and TiN top electrode, the partial breakdown of conducting filaments happens near TiN top electrode. By using the same reset stop voltage, experimental results in Figure 6 indicate that S3 has more defect traps in the filament rupture region due to Al doping effect [25]. Higher Al concentration near TiN top electrode guarantees easier and more uniform filament formation. This fits the experimental results very well. Easier filament formation explains the result that S2 and S3 show lower R_{LRS} than S1 (Figure 6). Improved uniformity explains narrower parameter dispersion of S2 and S3 compared with

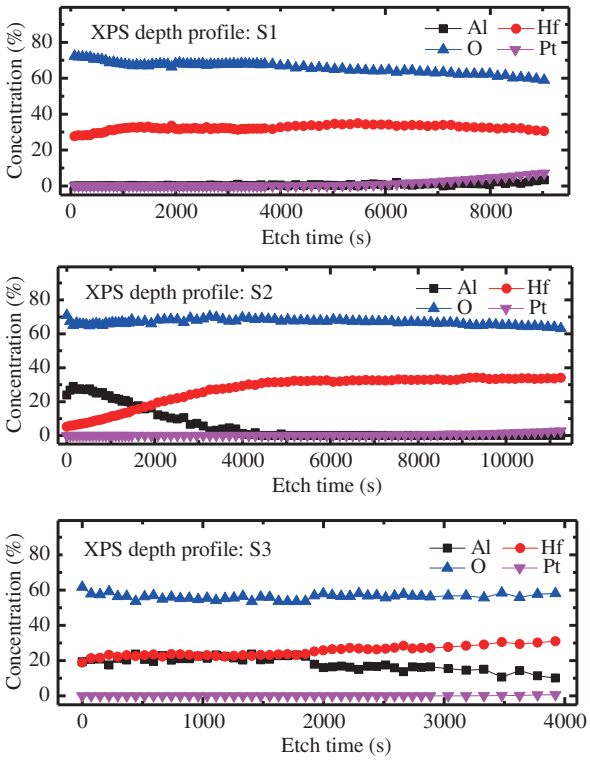

Figure 9 XPS depth profile of the samples supporting the proposed model.

S1. An exception is that S1 and S2 have similarly wide R_{LRS} distribution compared with S3, this may be resulting from a relatively longer rupture length of S2 which leads to non-uniformity during filament rebuilding (set) process. Above results are in good agreement with the model in literature that resistive switching is due to the partial rupture and reconstruction of conducting filaments [26] facilitated by Al atoms [15].

XPS depth analysis of the dielectric layer confirms the different doping profiles in the samples as illustrated in Figure 9. The dielectric layer etching process was terminated when significant Pt signal was detected. The results show that Al atoms are not detected near the surface in S1. In contrast Al atoms and Pt atoms are detected after 8000 s' etching, confirming the fact that in S1 Al atoms stay near bottom electrode. However, in S2 and S3 Al atoms are significantly detected near dielectric layer surface. S3 has a relatively wider Al-rich area compared with S2, while S2 has its Al-rich area only near surface. XPS results are in good agreement with the speculated doping profile in aforementioned model.

4 Summary

The impacts of doping profile on the switching properties of HfO_x based RRAM devices are studied in this work. Improved resistive switching uniformity is achieved. The effects of AlO_x insert layer and HfO_x film thickness are investigated by electrical measurements and XPS depth analysis to explain the enhanced performance. This work introduces a detailed doping profile modification approach of the optimization of HfO_x based resistive switching device, providing insights for highly reliable RRAM designs and helps understand RRAM switching mechanisms.

Acknowledgements

This work was supported by National Basic Research Program of China (973 Program) (Grant No. 2011CBA00600), National National Science Foundation of China (Grant Nos. 61376084, 61421005, 61334007) and National Science and Technology Major Project (Grant No. 2011ZX02708). The authors would like to thank the

State Key Laboratory of Micro&Nano Fabrication Technology, Peking University for device fabrication.

References

1 Baek I G, Lee M S, Seo S, et al. Highly scalable nonvolatile resistive memory using simple binary oxide driven by asymmetric unipolar voltage pulses. In: Proceedings of IEEE International Electron Devices Meeting, San Francisco, 2004. 587–590

2 Meijer G I. Materials science—who wins the nonvolatile memory race? Science, 2008, 319: 1625–1626

3 Waser R, Aono M. Nanoionics-based resistive switching memories. Nat Mater, 2007, 6: 833–840

4 Chen F T, Lee H, Chen Y S, et al. Resistance switching for RRAM applications. Sci China Inf Sci, 2011, 54: 1073–1086

5 Lee H Y, Chen Y S, Chen P S, et al. Evidence and solution of over-RESET problem for HfOX based resistive memory with sub-ns switching speed and high endurance. In: Proceedings of IEEE International Electron Devices Meeting, San Francisco, 2010. 19.7.1–19.7.4

6 Kim M J, Baek I G, Ha Y H, et al. Low power operating bipolar TMO ReRAM for sub 10 nm era. In: Proceedings of IEEE International Electron Devices Meeting, San Francisco, 2010. 19.3.1–19.3.4

7 Wong H S P, Lee H Y, Yu S M, et al. Metal oxide RRAM. Proc IEEE, 2012, 100: 1951–1970

8 Goux L, Degraeve R, Govoreanu B, et al. Evidences of anodic-oxidation reset mechanism in TiN/NiO/Ni RRAM cells. In: Proceedings of IEEE Symposium on VLSI Technology, Honolulu, 2011. 24–25

9 Chien W C, Chen Y R, Chen Y C, et al. A forming-free WOX resistive memory using a novel self-aligned field enhancement feature with excellent reliability and scalability. In: Proceedings of IEEE International Electron Devices Meeting, San Francisco, 2010. 19.2.1–19.2.4

10 Bersuker G, Gilmer D C, Veksler D, et al. Metal oxide RRAM switching mechanism based on conductive filament microscopic properties. In: Proceedings of IEEE International Electron Devices Meeting, San Francisco, 2010. 19.6.1–19.6.4

11 Ahn S E, Lee M J, Kang B S, et al. Investigation for resistive switching by controlling overflow current in resistance change nonvolatile memory. IEEE Trans Nanotechnol, 2012, 11: 1122–1125

12 Son J Y, Shin Y H. Direct observation of conducting filaments on resistive switching of NiO thin films. Appl Phys Lett, 2008, 92: 222106

13 Szot K, Speier W, Bihlmayer G, et al. Switching the electrical resistance of individual dislocations in single-crystalline $SrTiO_3$. Nat Mater, 2006, 5: 312–320

14 Wang Y, Liu Q, Long S B, et al. Investigation of resistive switching in Cu-doped HfO_2 thin film for multilevel non-volatile memory applications. Nanotechnol, 2010, 21: 045202

15 Yu S M, Gao B, Dai H B, et al. Improved uniformity of resistive switching behaviors in HfO_2 thin films with embedded Al layers. Electrochem Solid State Lett, 2010, 13: H36–H38

16 Long B M, Mandal S, Livecchi J, Jha R. Effects of mg-doping on HfO_2-based ReRAM device switching characteristics. IEEE Electron Dev Lett, 2013, 34: 1247–1249

17 Xie H W, Liu Q, Li Y T, et al. Nitrogen-induced improvement of resistive switching uniformity in a HfO2-based RRAM device. Semicond Sci Technol, 2012, 27: 125008

18 Xu N, Liu L F, Sun X, et al. Characteristics and mechanism of conduction/set process in TiN/ZnO/Pt resistance switching random-access memories. Appl Phys Lett, 2008, 92: 232112

19 Zhang H W, Gao B, Yu S, et al. Effects of ionic doping on the behaviors of oxygen vacancies in HfO_2 and ZrO_2: a first principles study. In: Proceedings of IEEE International Conference on Simulation of Semiconductor Processes and Devices, San Diego, 2009. 155

20 Yamamoto K, Hayashi S, Niwa M, et al. Electrical and physical properties of HfO_2 films prepared by remote plasma oxidation of Hf metal. Appl Phys Lett, 2003, 83: 2229

21 Lampert M A, Mark P. Current Injection in Solids. New York: Academic, 1970

22 Xia Y D, He W Y, Chen L, et al. Field-induced resistive switching based on space-charge-limited current. Appl Phys Lett, 2007, 90: 022907

23 Dong R, Lee D S, Xiang W F, et al. Reproducible hysteresis and resistive switching in metal-CuxO-metal heterostructures. Appl Phys Lett, 2007, 90: 042107

24 Fujimoto M, Koyama H, Konagai M, et al. TiO2 anatase nanolayer on TiN thin film exhibiting high-speed bipolar resistive switching. Appl Phys Lett, 2006, 89: 223509

25 Huang P, Liu X Y, Li W H, et al. A physical based analytic model of RRAM operation for circuit simulation. In: Proceedings of IEEE International Electron Devices Meeting, San Francisco, 2012. 26.6.1–26.6.4

26 Gao B, Kang J F, Chen Y S, et al. Oxide-based RRAM: unified microscopic principle for both unipolar and bipolar switching. In: Proceedings of IEEE International Electron Devices Meeting, Washington DC, 2011. 17.4.1–17.4.4